JOURNAL OF SOLID STATE CHEMISTRY **141,** 241–247 (1998)
ARTICLE NO. SC987974

Structural Studies of the Fast Oxygen Ion Conductor BICOVOX.15 by Single-Crystal Neutron Diffraction at Room Temperature

C. Muller,* M. Anne,*,[1] M. Bacmann,* and M. Bonnet†

*Laboratoire de Cristallographie, CNRS, BP 166X, 38042 Grenoble Cedex 09, France; and †DRFMC/SPSMS-MDN, Commissariat à l'Energie Atomique de Grenoble, 17 rue des Martyrs, 38054 Grenoble Cedex 09, France

Received February 2, 1998; in revised form July 10, 1998; accepted July 23, 1998

The room temperature crystal structure of the fast oxygen ion conductor $Bi_4(V_{0.85}Co_{0.15})_2O_{11-\delta}$ (BICOVOX.15) was refined within the average tetragonal unit cell from single-crystal neutron diffraction data. The unit cell dimensions are $a_T = 3.929(2)$ Å and $c_T = 15.476(9)$ Å in space group *I4/mmm* with $Z = 1$. The conventional R_w factor is 0.067. The structure consists of intergrowth, along the c-axis, of alternating $(Bi_2O_2)^{2+}$ sheets and $(VO_{3.5}\square_{0.5})^{2-}$ oxygen-deficient perovskite-like layers. The compound, which exhibits a high ionic conductivity at moderate temperatures, undergoes a phase transition around 780 K between the disordered high-temperature γ-phase and the lower temperature γ′-phase, showing a modulated superstructure. Oxygen vacancies are localized in the perovskite-like layers, oxygen stoichiometry is derived, and oxygen diffusion paths are proposed for the γ′-phase at room temperature. © 1998 Academic Press

INTRODUCTION

The compound $Bi_4(V_{0.85}Co_{0.15})_2O_{11-\delta}$ (BICOVOX.15) is a cobalt-doped form of $Bi_4V_2O_{11}$. It is among the best oxygen ion conducting materials (1–3) and belongs to the well-known BIMEVOX family whose structure is derived from the Aurivillius phase Bi_2MoO_6. The structural arrangement of $Bi_4V_2O_{11}$ is described as intergrowth, along the **c**-axis, of alternating $(Bi_2O_2)^{2+}$ sheets and $(VO_{3.5}\square_{0.5})^{2-}$ oxygen-deficient perovskite-like layers (Fig. 1) (4). Numerous metals (ME) have been substituted for vanadium and have been found to stabilize, at room temperature, a γ-type $Bi_4V_2O_{11}$ phase (γ′), the most symmetric crystallographic polymorph of $Bi_4V_2O_{11}$.

Like many of the doped forms, BICOVOX.15 undergoes a transition around 780 K between the high-temperature disordered γ-phase and the lower temperature γ′-phase. The γ-phase, whose structure has already been reported elsewhere (4, 5), crystallizes in the tetragonal system with unit cell parameters $a_T \approx 3.96$ Å and $c_T \approx 15.55$ Å, space group *I*4/*mmm*. On the other hand, both neutron and X-ray diffraction patterns of the γ′-phase exhibit weak commensurate modulations. They are due to the existence of ordered domains, showing a modulated superstructure in a tetragonal disordered γ-phase-like lattice (3). These modulations are described in the multiple cell $\mathbf{a} = \mathbf{a}_T - \mathbf{b}_T$, $\mathbf{b} = \mathbf{a}_T + \mathbf{b}_T$, $\mathbf{c} = \mathbf{c}_T$ by the propagation vector $\mathbf{q} = \frac{1}{3}(m\mathbf{a}^* + n\mathbf{b}^*)$, where m and n are integers. The first step for a full analysis of this structure is the determination and the refinement of the average structural model, excluding the superlattice reflections. This has already been done successfully on this type of compound in previous partial single-crystal structure refinements from X-ray data (2, 6–8). However, the relatively low electron densities of the oxygen atoms prevented the authors from determining atomic composition and vacancies. Here, the use of single-crystal neutron diffraction data increases the oxygen scattering contribution to diffraction intensities, thus making it possible to better localize the oxygen ions.

In this paper the crystallographic results of this new study are presented, together with the interpretation of Fourier synthesis maps from which the oxygen diffusion paths are inferred. They will then be used later in specific dynamic models explaining the high ionic conductivity observed in this compound.

EXPERIMENTAL

Single crystals were synthesized from a mixture of Bi_2O_3 (Ventron, 99.8%), V_2O_5 (Aldrich, 99.6%), and CoO (Aldrich) oxides in proportions respecting the $Bi_4(V_{0.85}Co_{0.15})_2O_{11-\delta}$ formula. An oscillating thermal cycle was applied to the mixture, carefully ground and placed in a gold crucible, to favor the growth of large crystals (3). The resulting single crystals are platelet shaped with the largest faces perpendicular to the **c** crystallographic axis. The chemical composition was controlled by energy-dispersive spectroscopy (EDS) coupled to a scanning electron microscope. From $Bi_4V_2O_{11}$ and Co-metal standards, the V/Co substitution rate was estimated to be 12%.

[1]To whom correspondence should be addressed. E-mail: anne@polycnrs-gre.fr

0022-4596/98 $25.00

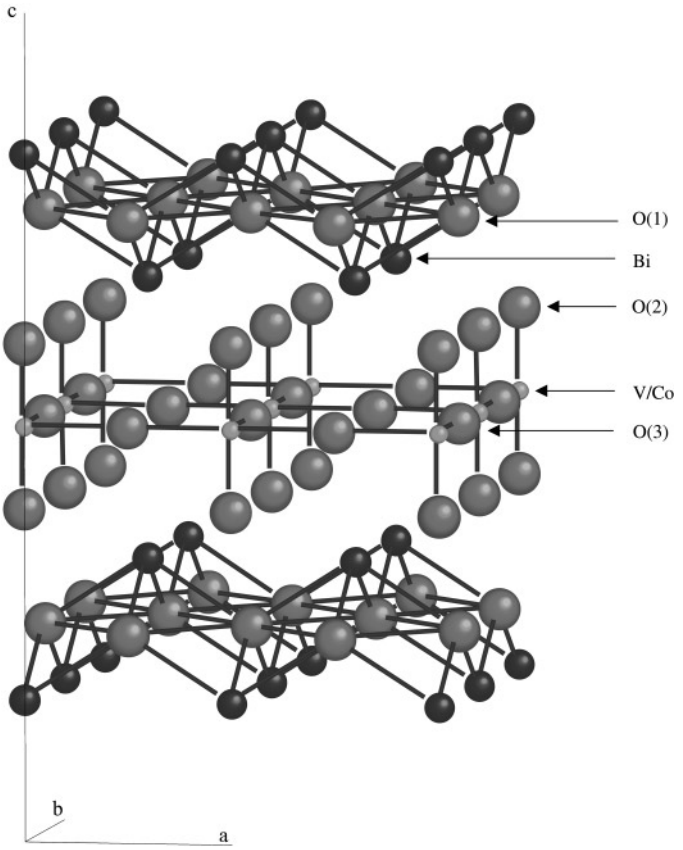

FIG. 1. Idealized structure of BICOVOX.15.

Neutron diffraction intensities were collected at room temperature on a single crystal of 4 mm^3 selected from the batch, using the DN4 four-circle diffractometer at the Silöe Reactor (CEA, Grenoble) and the neutron wavelength was $\lambda = 1.1811$ Å. The whole data collection (including the superlattice reflections) was carried out on the multiple tetragonal cell, which is more convenient to describe the modulated superstructure. However, as the crystal structure refinements are performed within the average cell, indexation of the main reflections was transformed into the twice smaller body-centered tetragonal unit cell. The cell parameters, $a_T = 3.929(2)$ Å and $c_T = 15.476(9)$ Å, were obtained by least-squares refinements from the diffraction angles of 24 Bragg reflections ($11^\circ \leq \theta \leq 29^\circ$).

A total of 591 main reflections were measured in the ω scan mode ($2^\circ \leq \theta \leq 45^\circ$), and 473 in the ω–2θ scan mode ($40^\circ \leq \theta \leq 60^\circ$).

The starting crystallographic model is described in the space group $I4/mmm$, in accordance with the limiting conditions for possible reflections.

The small neutron absorption cross-sections of the Bi, V, Co, and O atoms do not require absorption correction, the linear absorption coefficient μ being equal to 0.041 cm^{-1}. The percentage of the isotropic extinction correction applied (9) was less than 5%, except for three strong reflections ($\approx 10\%$).

Refinements by least squares against $|F_o|^2$ were performed using the MXD program implemented on an Alpha computer (10).

Crystallographic and experimental data are summarized in Table 1.

TABLE 1
Experimental Details

Crystal data	
Formula	$Bi_4(V_{0.85}Co_{0.15})_2O_{11-\delta}$
Crystal system	Tetragonal
Space group	$I4/mmm$ (No. 139)
a_T (Å)	3.929(2)
c_T (Å)	15.476(9)
V_T (Å^3)	238.9(4)
Z	1
Molecular weight (g mol^{-1})	1109.0
Density	7.8
μ (cm^{-1})	0.041
Morphology	Platelets
Color	Black
Volume (mm^3)	4
Data collection	
Temperature (K)	293
Wavelength (Å)	1.1811
Scan modes	ω scan and ω–2θ scan
Maximum Bragg angle θ (deg)	60
Coherent scattering lengths	
b_{Bi} (10^{-12} cm)	0.853
b_O (10^{-12} cm)	0.580
b_V (10^{-12} cm)	−0.040
b_{Co} (10^{-12} cm)	0.249
Structure refinement	
Refinement type	F^2
Reflections for cell refinement	24 with $11^\circ \leq \theta \leq 29^\circ$
Measured reflections	591 with $2^\circ \leq \theta \leq 45^\circ$ (ω scan)
	473 with $40^\circ \leq \theta \leq 60^\circ$ (ω–2θ scan)
Total measured reflections	1064
Independent reflections	137
Reflections used	137
Parameters refined	31
Weighting scheme	$w = 1/\sigma^2$
$R(F^2)$	0.048
$R_w(F^2)$	0.067

STRUCTURE REFINEMENT

The so-called "idealized model" (Table 2) which corresponds to the crystallographic structure of the parent Bi_2MoO_6 compound (4, 11) was first tested but the accuracy of the refinements was very poor. In fact, difference Fourier syntheses calculated from the results show considerable

TABLE 2
Idealized Atomic Positions Described in the *I4/mmm* Space Group

Atom	Site	Occupancy factor	Normalized multiplicity[a]	x	y	z
Bi	4*e*	1.0	0.125	0	0	0.17
V/Co	2*b*	1.0	0.0625	0	0	$\frac{1}{2}$
O(1)	4*d*	1.0	0.125	0	$\frac{1}{2}$	$\frac{1}{4}$
O(2)	4*e*	1.0	0.125	$\frac{1}{2}$	$\frac{1}{2}$	0.10
O(3)	4*c*	1.0	0.125	$\frac{1}{2}$	0	0

[a]The site multiplicity is normalized to the multiplicity of the 32*o* general position of the space group *I*4/*mmm*.

TABLE 3
Refined Atomic Positions and Occupancies

Atom	Site	Occupancy factor × normalized multiplicity[a]	x	y	z
Bi	4*e*	0.125	0	0	0.1691(1)
V	2*b*	0.0522(6)	0	0	$\frac{1}{2}$
Co	2*b*	0.0078	0	0	$\frac{1}{2}$
Bi	2*b*	0.0025(6)	0	0	$\frac{1}{2}$
O(1)	4*d*	0.125	0	$\frac{1}{2}$	$\frac{1}{4}$
O(21)	4*e*	0.019(4)	$\frac{1}{2}$	$\frac{1}{2}$	0.109(2)
O(22)	16*n*	0.095(8)	$\frac{1}{2}$	0.331(5)	0.092(1)
O(31)	4*c*	0.025(7)	$\frac{1}{2}$	0	0
O(32)	16*n*	0.068(9)	$\frac{1}{2}$	0.055(6)	0.038(1)

[a]The site multiplicity is normalized to the multiplicity of the 32*o* general position of the space group *I*4/*mmm*.

broad and elongated residual nuclear densities around some oxygen sites of the ideal structure. Such densities can be formally described by splitting of the crystallographic sites and/or by an anharmonic development of the atomic displacement parameters. This is usual for a fast ion conductor in which some species is diffusing throughout the structure, with a probability density function (pdf) which is not isotropic around one well-defined site.

In the case of the BICOVOX compound, the anharmonicity effect does not seem to be very visible as it would have been emphasized by the behavior of the mean-square displacements of oxygen atoms versus the temperature. Therefore, only splitting of the ideal sites was used for the structure determination. The atomic description of the crystallographic model and the different steps of the refinements are developed in the following.

At the beginning of the refinements, the occupancies of all but the Bi site (assumed fully occupied) were simultaneously refined with the position parameters and an overall atomic displacement parameter to get a good initial approximation for the occupancies. The atomic positions were then refined together with the anisotropic atomic displacement parameters, the occupancies remaining fixed. The final step consisted of the simultaneous refinement of the occupancies, the atomic positions, and the anisotropic atomic displacements, except for the strongly correlated oxygen atoms in the perovskite-like layers.

The refined atomic positions and the occupancies are given in Table 3, and the atomic displacement parameters are summarized in Table 4.

$(Bi_2O_2)^{2+}$ *Sheets*

Bismuth and oxygen atoms of the $(Bi_2O_2)^{2+}$ sheets were respectively located on well-defined 4*e* and 4*d* sites. Anisotropic atomic displacement parameters were refined for each site and occupancy for the oxygen site only. A full occupancy was assumed during the last stage of the refinements, since the value of the corresponding parameter reaches 1, within the uncertainty. Furthermore, the resulting atomic displacement parameters are almost isotropic.

Perovskite-like Layers

In the idealized model, vanadium and cobalt atoms share the 2*b* site with occupancies in agreement with the chemical formula. However, Fourier difference syntheses have revealed a residual nuclear density which could be compensated by a high and unrealistic cobalt occupancy given the initial chemical composition. This extranuclear density can be readily explained by the presence of a very small amount of bismuth on this site, as reported in the BICOVOX solid solution diagram in Ref. 2. In fact, the nuclear density is very sensitive to atoms with large neutron scattering lengths such as bismuth.

Thus, considering that some bismuth shares the vanadium site together with the cobalt, the V/Bi occupancy was refined assuming (i) a 12.5% realistic substitution rate of cobalt, which is in agreement with the EDS analysis, and (ii) an absence of vacancies on this site. The atomic displacements are described by the same isotropic parameter U_{iso} and its very low refined value obtained is probably due

TABLE 4
Isotropic and Anisotropic Atomic Displacement Parameters

Atom	U_{iso} (Å^2)	U_{11} (Å^2)	U_{22} (Å^2)	U_{33} (Å^2)	U_{12} (Å^2)	U_{13} (Å^2)	U_{23} (Å^2)
Bi		0.0304(7)	U_{11}	0.0215(8)	0	0	0
V/Co/Bi	0.007(14)						
O(1)		0.0178(7)	U_{11}	0.036(1)	0	0	0
O(21)		0.06(2)	U_{11}	0.0008(90)	0	0	0
O(22)		0.069(7)	0.07(2)	0.067(7)	0	0	0.03(1)
O(31)		0.09(3)	− 0.009(13)	0.32(9)	0	0	0
O(32)		0.05(1)	0.09(2)	0.08(2)	0	0	0.07(2)

[a]*Note.* The anisotropic atomic displacement factor exponent takes the form $-2\pi^2[h^2a^{*2}U_{11} + \cdots + 2klb^*c^*U_{23}]$.

to the different types of atoms on the same crystallographic site.

Fourier difference syntheses also revealed elongated nuclear densities around the O(2) and O(3) oxygen sites, showing a considerable atomic disorder. To better model these nuclear densities and thus determine the oxygen occupancies, one oxygen atom was placed on the idealized site and another off this site (both with partial site occupancy). After several attempts, the best description was obtained using the following sites:

Around O(2): The O(21) oxygen atom was set on a 4*e* site, In addition, the distorted nuclear density around this idealized position was described by another oxygen atom O(22), placed off the fourfold axis, on a 16*n* site.

Around O(3): The O(31) oxygen atom was set on a 4*c* site, and the residual nuclear density around this site was described by the O(32) atom on a 16*n* site.

Anisotropic atomic displacement parameters and occupancies were refined for all these atoms. The correlation coefficients are in the range 0.35–0.85, which is acceptable for such an atomic description.

At the end of the refinements, the O(22) oxygen atom has moved away, along *y* and *z*, from the idealized position described by the O(21) oxygen atom. The O(32) oxygen atom was also shifted from the idealized O(31) position, along *y* and *z*. Figure 2 shows the atomic distribution used to model the nuclear densities around the vanadium site. This local arrangement around the V site is very close to the one obtained by Abrahams *et al.* in quenched γ-BICOVOX from combined neutron and X-ray powder diffraction data (5).

The atomic displacement parameters are generally high for these sites, especially the U_{33} parameter of the O(31) atom, which takes into account the elongated nuclear density along the $\mathbf{c}_T$ axis. The U_{22} negative component of the O(31) atom is due to the strong correlation with that of O(32), and this illustrates the difficulty in modeling disordered atom distributions in a fast ionic conductor compared to a conventional crystallographic structure.

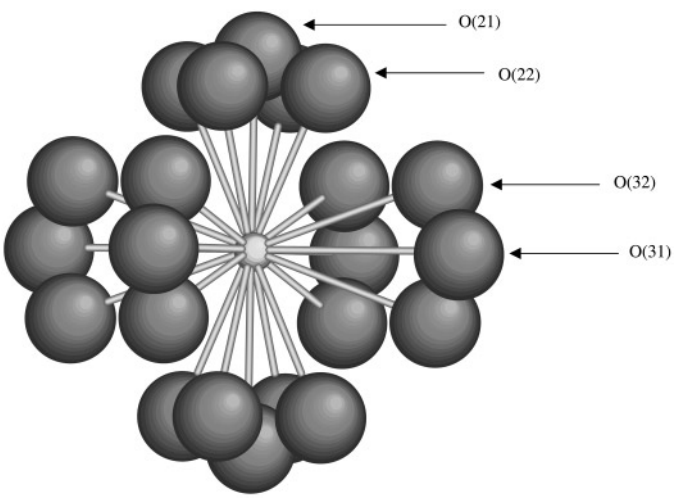

FIG. 2. Distribution of the oxygen atoms around the V/Co/Bi site in the average structure.

DISCUSSION

Bismuth Environment

From the structure refinement results, it is observed that the bismuth and oxygen atoms of the $(Bi_2O_2)^{2+}$ sheets have relatively isotropic atomic displacement parameters and chemical occupancies equal or almost equal to 1. The Bi–O(1) distance of 2.330(1) Å (Table 5) corroborates the rigidity of these non-oxygen-deficient sheets. The observed Fourier map presented in Fig. 3 shows actually the regular features of the nuclear densities around these atoms, which do not favor oxygen diffusion through these sheets.

Therefore this rigidity explains the strong electrical anisotropy observed on the conductivity curves (Fig. 4) (3). The electrical conductivity measured parallel to the ($\mathbf{a}_T$, $\mathbf{b}_T$) plane (referred to as $\sigma_{//}$) is one or two orders of magnitude higher than that measured perpendicularly to the plane (referred to as $\sigma_{\perp}$). This anisotropy has already been observed in previous work (11, 12), and especially in the BICOVOX compounds (3, 13, 14).

Partial Substitution of Bismuth on the Vanadium Site and Oxygen Stoichiometry

The Fourier map in the vanadium-containing ($\mathbf{a}_T$, $\mathbf{b}_T$) plane shows strong nuclear density at the V site (Fig. 5), despite the small coherent scattering of the vanadium. As mentioned earlier this extra density is easily compensated if a small amount of bismuth shares the vanadium site together with the cobalt. Refinement of the Bi occupancy on this site indicates a partial V/Bi substitution rate of about

TABLE 5
Selected Interatomic Distances (Å)

$(Bi_2O_2)^{2+}$ sheets	
Bi–O(1)	2.330(1)
O(1)–O(1)	2.778(1)
Bi–Bi	3.929(2)
	3.740(2)
Perovskite-like layers	
V/Co/Bi–O(21)	1.687(30)
V/Co/Bi–O(22)	1.571(15)
V/Co/Bi–O(31)	1.965(1)
V/Co/Bi–O(32)	1.845(5)
O(21)–O(31)	2.589(20)
O(31)–(31)	2.778(1)

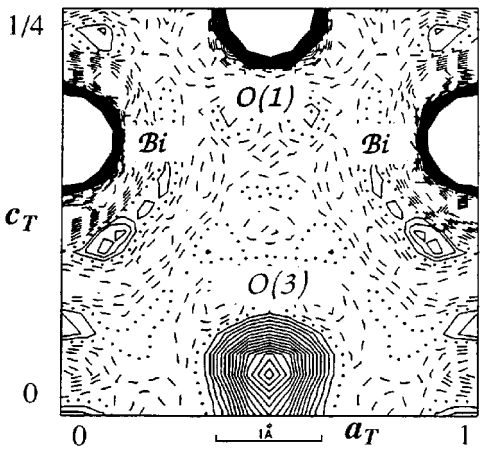

FIG. 3. Fourier map of the ($\mathbf{a}_T$, $\mathbf{c}_T$) crystallographic plane (at $y = 0$), showing the nondispersed nuclear densities around the bismuth and O(1) oxygen sites of the $(Bi_2O_2)^{2+}$ sheets.

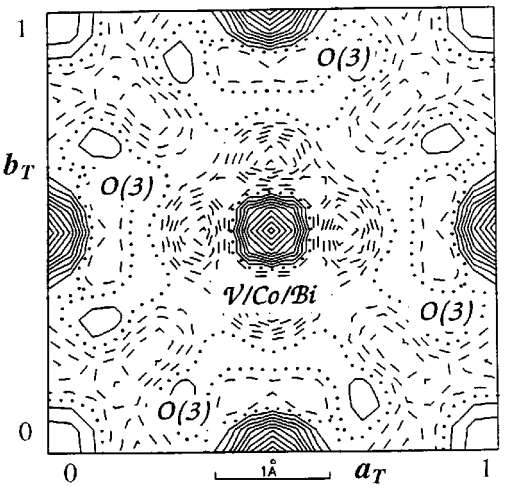

FIG. 5. Fourier map of the ($\mathbf{a}_T$, $\mathbf{b}_T$) crystallographic plane (at $z = 0$), showing the strong nuclear density at the vanadium site.

4%, with the hypothesis of a 12.5% V/Co substitution rate derived from the starting chemical composition. This result is to be related to the ternary phase diagram proposed by Lazure *et al.*, in which it is reported that syntheses carried out from a stoichiometric mixture of the reagents Bi_2O_3, V_2O_5, and CoO give a Bi-rich phase. Furthermore, under these conditions the partial substitution rate of the bismuth on the vanadium site was estimated to be 4% (2). Thus, the refinement results fully corroborate the partial V/Bi substitution previously suggested.

The chemical formula of the compound, deduced from the refinements, can be written as $Bi_4(V_{0.835}Co_{0.125}Bi_{0.04})_2O_{11-\delta}$, where the number of oxygen atoms must respect the chemical electroneutrality (V^{5+}, Co^{2+}, and Bi^{3+} cations) which imposes that $(11 - \delta) = 10.545$.

On the other hand, the oxygen occupancies around the O(2) and O(3) sites were accurately determined using the above detailed model describing the complex nuclear densities (Table 3). The sum of the O(21) and O(22) site occupancy factors has to be compared to the full occupancy of the O(2) site in the idealized structural model (Table 2). Thus, the total occupancy fraction near the O(2) site is equal to $0.114/0.125 = 0.912$. Accordingly, the occupancy fraction near the idealized O(3) site involves the sum of the O(31) and O(32) site occupancy factors and is equal to: $0.093/0.125 = 0.744$. The oxygen vacancy rates deduced from these values are 8.8% around the O(2) site and 25.6% around the O(3) site. This result corroborates the vacancy distribution proposed in quenched γ-BICOVOX by Abrahams *et al.* (5).

Furthermore, the addition of all the refined oxygen occupancies gives a total number of $(11 - \delta) = 10.62(25)$ oxygen atoms per unit cell formula, which is in excellent agreement, within the uncertainties, with the number deduced from the electroneutrality relationship.

All the preceding refinement results obtained at room temperature can be summarized in the following way. The whole crystallographic structure of this fast oxygen ion conductor BICOVOX.15 is composed of alternating non-oxygen-deficient sheets, formed by the $(Bi_2O_2)^{2+}$ rigid sublattice, and oxygen-deficient perovskite-like layers, formed by the $(VO_{3.5}\square_{0.5})^{2-}$ disordered and delocalized anion sublattice. In the latter, the proportion of oxygen vacancies around the O(3) equatorial site is three times as high as around the O(2) apical one.

This structural arrangement explains the observed bi-dimensional oxygen diffusion and the low conductivity value measured along the **c** crystallographic axis.

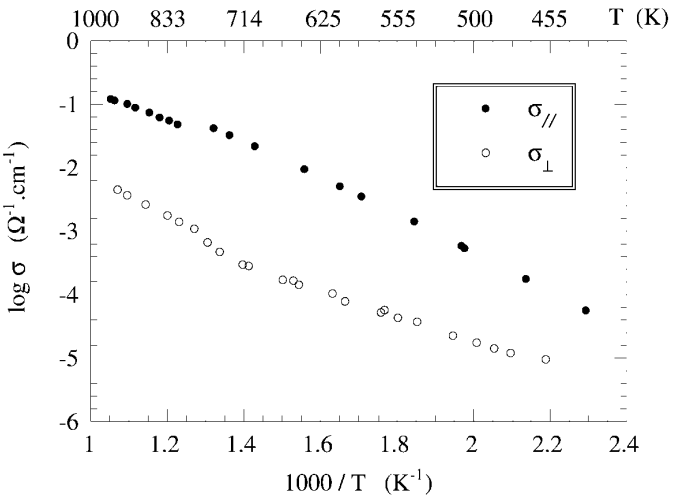

FIG. 4. Electrical conductivity measurements on single crystals: $\sigma_{//}$ and $\sigma_{\perp}$ are the conductivities measured respectively parallel and perpendicular to the $(Bi_2O_2)^{2+}$ sheets.

Oxygen Diffusion Paths

The scattering density of the vibrating atom is related to the probability density function through the thermal displacements. In this way, connected elongated nuclear densities observed in the case of ionic conductors can be associated with the existence of diffusive motions. Therefore, a goal of this structure determination was to find such nuclear densities. In actual fact, realistic diffusion paths for the oxygen were inferred after a careful inspection of Fourier syntheses calculated from the observed intensities and the refined phases. Figure 6 presents a Fourier map of the ($\mathbf{a}_T$, $\mathbf{c}_T$) crystallographic plane (at $y = \frac{1}{2}$). This map clearly exhibits elongated nuclear densities around the O(2) and O(3) sites, which describe circle-like diffusion paths connecting the two sites.

These diffusion paths exist only along the $\mathbf{a}_T$ and $\mathbf{b}_T$ crystallographic axis directions. Outside these directions, small and limited residual nuclear densities were observed as in Fig. 7 for example.

The O(21)–O(31) distances, 2.589(20) Å, are shorter than the smallest O(31)–O(31) ones, 2.778(1) Å (Table 5), and there are no elongated densities connecting the latter. Therefore, assuming these results can be transposed in the real modulated structure, it is unlikely that the diffusion occurs between the O(3) sites. A more favorable diffusion path involves the O(2) apical oxygen atoms, together with the O(3) equatorial ones. In that case, the O(2) site acts as a short bridge connecting two O(3) sites. These results are in agreement with the migration pathways deduced from the calculations of interatomic potentials in Bi_2WO_6 (15).

The fast local motion, studied elsewhere by neutron coherent quasielastic scattering (3, 16), can be explained by this exchange of oxygen atoms between the split O(2) and O(3) sites. The most probable diffusion model consists of a uniaxial rotation of oxygen anions over a circle, the rotation axis being parallel to the $\mathbf{a}_T$ and $\mathbf{b}_T$ crystallographic axes. The diffusion circles being connected by the O(2) and O(3) sites, the oxygen anions may jump from one circle to a neighboring one, giving rise to the long-range motion observed by neutron scattering (3, 16).

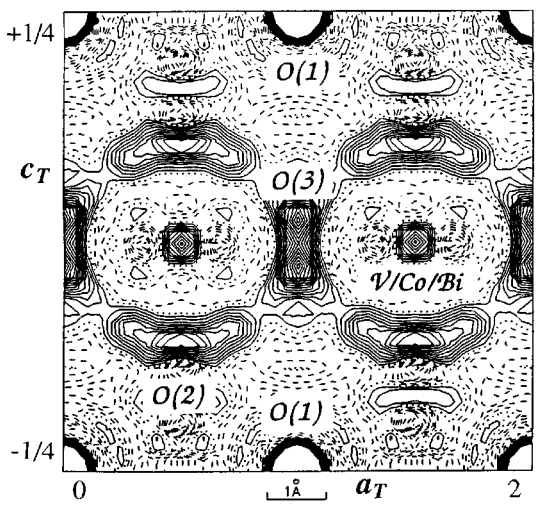

FIG. 6. Fourier map of the ($\mathbf{a}_T$, $\mathbf{c}_T$) crystallographic plane (at $y = \frac{1}{2}$), showing circle-like oxygen diffusion paths.

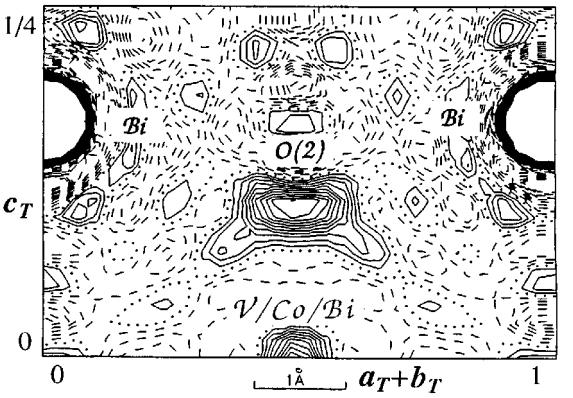

FIG. 7. Fourier map of the ($\mathbf{a}_T + \mathbf{b}_T$, $\mathbf{c}_T$) crystallographic plane which contains the vanadium site.

CONCLUSION

The structure refinement of the BICOVOX.15 compound reported here in the average unit cell is the first step of a more general study of the diffusion mechanism in this fast oxygen ion conductor. This structure determination was essential to be able to propose a static geometric arrangement of the oxygen anions to be fed in the dynamic scattering law, which will be adjusted to the coherent quasielastic neutron scattering data.

ACKNOWLEDGMENT

The authors thank Professor J. Fouletier from the Laboratoire d'Electrochimie et de Physicochimie des Matériaux et des Interfaces, Saint-Martin d'Hères France, who performed the electrical conductivity measurements on single crystals.

REFERENCES

1. G. Mairesse, *in* "Fast Ion Transport in Solids," (B. Scrosati *et al.*, Eds.), p. 271. Kluwer, Dordrecht, 1993.
2. S. Lazure, R. N. Vannier, G. Nowogrocki, G. Mairesse, C. Muller, M. Anne, and P. Strobel, *J. Mater. Chem.* **5,** 1395 (1995).
3. C. Muller, Thesis, Université J. Fourier, Grenoble, 1996.
4. F. Abraham, J. C. Boivin, G. Mairesse, and G. Nowogrocki, *Solid State Ionics* **40/41,** 934 (1990).

5. I. Abrahams, F. Krok and J. A. G. Nelstrop, *Solid State Ionics*, **90,** 57 (1996).
6. O. Joubert, Thesis, Université de Nantes, Nantes, 1993.
7. O. Joubert, A. Jouanneaux, M. Ganne, R. N. Vannier, and G. Mairesse, *Solid State Ionics* **73,** 309 (1994).
8. O. Joubert, M. Ganne, R. N. Vannier, and G. Mairesse, *Solid State Ionics* **83,** 199 (1996).
9. P. Becker and P. Coppens, *Acta Crystallogr., Sect. A* **30,** 129 (1974).
10. P. Wolfers, *J. Appl. Crystallogr.* **23,** 554 (1990).
11. E. Pernot, Thesis, Université J. Fourier, Grenoble, 1994.
12. E. Pernot, M. Anne, M. Bacmann, P. Strobel, J. Fouletier, R. N. Vannier, G. Mairesse, F. Abraham, and G. Nowogrocki, *Solid State Ionics* **70/71,** 259 (1994).
13. C. Muller, D. Chateigner, M. Anne, M. Bacmann, J. Fouletier, and P. de Rango, *J. Phys. D: Appl. Phys.* **29,** 3106 (1996).
14. S.-K. Kim and M. Miyayama, *Solid State Ionics* **104,** 295 (1997).
15. S. Lazure, Thesis, Université des Sciences et Technologies de Lille, Lille, 1996.
16. C. Muller, M. Anne, M. Ferrand, M. Bacmann, J. Fouletier, and P. Strobel, to be published.